Methanol Diffusion in Zeolite HY: A Combined Quasielastic Neutron Scattering and Molecular Dynamics Simulation Study

Alexander J. O'Malley,[ab] Victoria García-Sakai,[c] Ian P. Silverwood,[c] Nikolaos Dimitratos,[d] Stewart F. Parker,[bc] and C. Richard A. Catlow*[abd]

[a]*Department of Chemistry, Materials Chemistry, University College London, Third Floor, Kathleen Lonsdale Building, Gower Street, London, WC1E 6BT, UK. E-mail: c.r.a.catlow@ucl.ac.uk*

[b]*The UK Catalysis Hub, Research Complex at Harwell, Rutherford Appleton Laboratory, Oxfordshire, OX11 0FA, UK*

[c] *ISIS Facility, STFC Rutherford Appleton Laboratory, Chilton, Didcot, Oxfordshire, OX11 0QX, UK*

[d]*Cardiff Catalysis Institute, School of Chemistry, Cardiff University, CF10 3AT, UK*

The diffusion of methanol in zeolite HY is studied using tandem quasielastic neutron scattering (QENS) experiments and molecular dynamics (MD) simulations at 300-400 K. The experimental diffusion coefficients were measured in the range 2-5 x 10^{-10} m^2s^{-1} and simulated diffusion coefficients measured in the range of 1.6-3.2 x 10^{-9} m^2s^{-1}. Activation energies were measured as 8.8 and 6.9 kJ mol^{-1}using QENS and MD respectively. Differences may be attributed predominantly to the experimental use of a dealuminated HY sample, containing significant defects such as strongly adsorbing silanol nests, compared to a perfect simulated crystal containing only evenly distributed Brønsted acid sites. Experimental and simulated diffusivities measured in this study are lower than those obtained from those previously calculated in siliceous faujasite, due to methanol H-bonding to Brønsted acid sites as observed in the MD simulations. However, both experimental and simulated diffusivities were significantly higher than those obtained in NaX, due to the higher concentration of extraframework cations present in the previously studied structures.

1. Introduction

The behaviour of methanol in different zeolites is of great interest to a number of catalytic processes such as the methanol-to-hydrocarbons process[1-4] and the alkylation of aromatic hydrocarbons.[5] The faujasite structure on which zeolites Y and X are based, though primarily used for the fluid catalytic cracking of heavy oil fractions to lighter hydrocarbons,[6,7] has been studied for the side chain alkylation of aromatics with alkali metal substituted Y zeolites using methanol,[8,9] and the conversion of methanol to dimethylether.[10,11] Understanding any microporous catalytic process requires detailed knowledge of the diffusion behaviour of species confined in the catalyst. However, the unique structures associated with each zeolite topology mean that prediction of diffusion behaviour using quantitative theory is not possible. The study of transport properties, particularly using microscopic methods (concerned with direct measurement of molecular motion) has been applied both experimentally[12-17] and theoretically[18-26] to investigating molecular diffusion in faujasite zeolites. In particular, the potential for combined experimental and theoretical studies of these systems using complementary techniques such as quasielastic neutron scattering (QENS) and molecular dynamics (MD) simulations has been reported in a number of studies.[27] Recent work has shown how state-of-the-art MD simulations can obtain excellent agreement with experimentally measured diffusivities with QENS and neutron spin-echo techniques, and provide qualitative insight such as preferred siting of linear[28,29] and spherical sorbates in zeolites.[30]

Though an understanding of molecular diffusion as a function of zeolite topology is crucial for optimisation of a catalytic process, the composition such as the presence and concentration of counterions in the zeolite structure will also have a significant effect on molecular transport. Previous QENS studies have demonstrated this feature, observing that *n*-alkanes in MFI zeolites undergo slower diffusion by a factor of 3.8-5.2 when Na^+ counterions are present compared to the fully siliceous structure.[31,32] In terms of methanol, the adsorption behaviour has been studied showing strong coordination with Na^+ [33] in addition to a range of other counterions[34] and Brønsted acid sites[35] in faujasite zeolites. The significant interaction with these sites would be expected to hinder molecular diffusion through the structure.

Experimentally, diffusion studies of methanol in faujasite have been performed only using NaX, as the methods used require larger crystal sizes. A comparison of zero-length column (ZLC) and PFG-NMR methods showed good agreement in the activation energy (11 kJ mol^{-1}) upon extrapolation to zero loading.[36] The PFG-NMR measurements showed a maximum in diffusivity at a loading of 8 molecules per faujasite cage. Comparison between the two techniques is difficult, as traditional ZLC measurements are only suited to low concentrations. However, the tracer ZLC method allowed direct comparison at 100°C, giving results that agree with this trend in the variation with loading. [37]

Molecular dynamics simulations have also been used to study methanol diffusion in faujasites, without the crystal size constraint. Comparison between NaX (Si/Al = 2.4) and siliceous Y was made,[38] showing that the presence of counterions can significantly inhibit the diffusion (by a factor of 22 at higher temperatures) with an activation energy higher by a factor of 4 with the counterions present. The increase was attributed to a strong interaction between the methanol oxygen and the Na^+ counterion. Longer MD simulations[39] of this system found that activation energies for long range (intercage) motion decrease with loading, and that at lower loadings surface-mediated (intracage) diffusion dominates. Cation behaviour upon methanol adsorption was also studied,[40] showing that the extra-framework Na^+ in certain crystallographic sites can move to the centre of the supercage, hindering methanol motion upon interaction with the methanol. The cation mobility is also limited at higher methanol loadings. Later MD simulations incorporated this cation mobility, giving qualitative agreement with the experimentally observed diffusivity maximum at lower concentrations.[41]

To our knowledge, no studies have been reported measuring microscopically the diffusion of methanol in zeolite HY, though this zeolite has been studied for activity in methanol dehydration[42] and methanol-to-olefin transformations[43] post dealumination. As previously mentioned, study of higher silica faujasites is not feasible using methods such as PFG-NMR as they necessitate larger crystals, which are unavailable for these zeolites. This problem stems from the timescale of the experiment (µs to ms) during which a molecule may reach the edges of a small crystallite, restricting its diffusion and invalidating the use of the Stokes-Einstein equation in calculating the diffusivity. The QENS method, which measures movement over the nanoscale, does not suffer from this limitation, allowing intracrystalline

diffusion in sub-micron crystals to be quantified. Indeed, the QENS method has been applied to systems particularly relevant to the methanol-to-hydrocarbons process in ZSM-5, studying methanol dynamics[44,45] and motion of smaller[46] and larger hydrocarbons.[31,47-49]

In this paper, we report a combined experimental/theoretical microscopic study of methanol diffusivity in a commercial sample of zeolite HY (Si/Al = 30) using QENS experiments and MD simulations. We obtain acceptable agreement between the two techniques in measured and calculated self-diffusivities (D_s) when differences between the experimental sample and the modelled structure are taken into account, and find a logical trend in diffusivities when comparing with previous studies of siliceous faujasite and NaX when considering the differing concentration of coordination sites between studies.

2. Methodology

2.1 Quasielastic Neutron Scattering Experiments

The HY samples used were commercial zeolite catalysts obtained from Zeolyst International (CBV720, Si/Al ratio = 30) with the bulk crystallinity verified by powder X-ray diffraction in recent studies.[50,51] The zeolite HY samples were received in the catalytic protonated form, already steam dealuminated to this composition. The samples were dehydrated at 120˚C under flowing helium for 4 hours. After cooling to room temperature, methanol was then loaded using He as a carrier gas to a loading of 6 molecules per unit cell. The samples (4.5 grams in total) were transferred inside a glovebox under argon to thin walled aluminium containers of annular geometry. All measurements were performed using the time-of-flight backscattering neutron spectrometer OSIRIS[52] at the ISIS Pulsed Neutron and Muon Source. The cells were placed in a top-loading closed cycle refrigerator, and a resolution measurement was taken at a base temperature of 6 K. QENS measurements were then taken at 300, 330, 360 and 400 K. Pyrolitic graphite 002 analyser crystals were used giving an energy resolution of 24.5 μeV with energy transfers measured in a window of ±0.55 meV, the detector covered measurements over a in a Q range of 0.2–1.5 Å^{-1}. The measurement was taken of an empty zeolite sample and the signal was then subtracted from the signal of the loaded zeolite, so that only the signal from the methanol could be extracted. In this way

any scattering from the aluminium container, which is very low in comparison with the empty zeolite is also subtracted. No further corrections were necessary. All QENS spectra were fitted using the neutron analysis software DAVE.[53]

2.2 Molecular Dynamics Simulations

2.2.1 The Zeolite HY Structure

The zeolite Y structure has cubic $Fd\bar{3}m$ symmetry.[54] Periodic boundary conditions were employed and a 2x2x2 supercell of 4609 atoms was used. Aluminium sites and charge compensating protons were added to match the ratio of Si/Al =30 and were located as far from each other as possible in accordance with Dempsey's rule[55] with the hydroxyl group protruding into the supercage. Full ionic charges were assigned to the framework species for all simulations, with the Coulombic summations being treated using the Ewald method. The supercell with dimensions of 48.49 Å in the Cartesian directions is depicted in figure 1.

A flexible model of the zeolite framework was used. There has been debate regarding the use of a flexible framework when the sorbate is significantly smaller than the pore aperture, and the influence of the force field used on the measured diffusivities. Examples of recent studies into the effect of pore breathing in diffusion of small molecules include a comprehensive study by Ghysels et al [56] of MTG relevant small molecules in small pore zeolites and SAPO structures, introducing a new descriptor (the accessible window area)

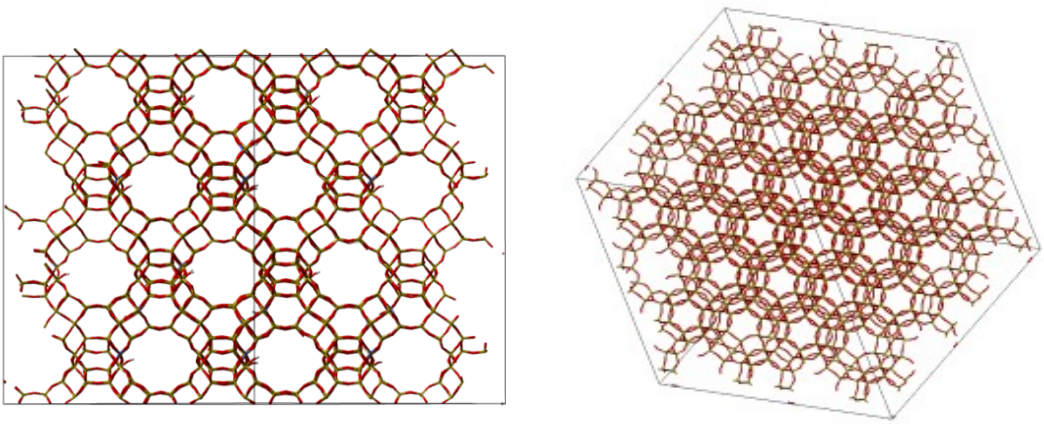

Fig 1. The 2x2x2 zeolite HY supercell used, viewed from (left) the 110 direction and (right) the 111 direction showing the structure of the faujasite cages. All experimental visualisations in this study were created using the visualisation software package Aten1.8.31.[49]

which correlated well with the number of ethene crossings of 8 membered ring windows in a number of structures. In the context of force field comparisons, Zimmerman et al. studied methane diffusion AFI, LTL and MTW zeolites comparing the general valence force field of Nicholas[57] with the Demontis[58] model which considers only interactions between nearest neighbours. They found that depending on the topology studied and loading used, the flexibility potentials can influence the results qualitatively as well as quantitatively, concluding that careful choice of the representative force field is necessary to improve on the rigid framework approximation. Garcia-Sanchez et al. [59] also concluded that diffusivities obtained depend very much on the force field used when comparing the Nicholas force field with that of Sauer and Hill [60] when studying methane diffusion in LTA zeolites. They found that at certain loadings the flexible Hill and Sauer model give higher diffusivities than the rigid framework approximation, with contradictory results obtained using the Nicholas model. It is therefore important when considering such framework flexibility that the chosen force field is suitable for the zeolite under study.

The potentials used to describe the flexible, acidic zeolite framework in the present work were taken from work studying acidic zeolite frameworks by Schröder *et* al [61] stemming mainly from empirical fitting to structural and physical properties of α-quartz and Al_2O_3 with additional fitting of the bridging hydroxyl groups to ab-initio data. These potential parameters have been widely used have been shown to reproduce structural and physical properties of faujasite zeolites well [62] and are thus considered appropriate for study of small molecule diffusion in this system. Parameters include a Buckingham potential to describe Si-O, Al-O and O-O interactions, along with a harmonic three-body potential to describe the O-Si-O and O-Al-O triads (listed in table 1), and a Morse potential describing the bond between the acidic proton and hydroxyl framework oxygen (O_b). A cut-off distance of 10 Å was used.[63]

2.2.2 Methanol Parameters

The intramolecular methanol potential parameters were taken from the work of Plant et al.[38] who modified those of Blanco and Auerbach[64] after Mulliken analysis of DFT calculations. The partial charges were tested by comparison of the simulated IR spectrum

with the corresponding experimental IR and gave good agreement,[65,66] the intramolecular methanol bond, angle and dihedral parameters were originally derived by fitting of *ab initio* data to millimeter wave spectroscopy [67,68] and electron diffraction.[69] The methanol-methanol interactions were adjusted from those in the CVFF[70] forcefield and are represented by a Lennard-Jones potential the parameters of which, along with the atomic charges and intramolecular bonding, angle and dihedral parameters are listed in table 2.

Zeolite-Zeolite Interactions			
Buckingham Potential			
Atoms	*A* (eV)	*ρ* (Å)	*C (eV Å^6)*
Si- -O	1283.907	0.32052	10.66158
Si- -O_b	983.5566	0.32052	10.66158
O- -O	22764.0	0.149	27.88
Al- -O	1460.3	0.29912	0
Al- -O_b	1142.6775	0.29912	0
O_b- -O	22764.0	0.149	27.88
O- -H_b	311.97	0.25	0
Morse Potential			
Atoms	*D* (eV)	α (Å^{-1})	r_0 (Å)
O_b- -H_b	7.0525	2.1986	0.9845
Three-body potential			
Atoms	*K* (eV rad^{-2})		θ(°)
O-Al-O/O_b	2.09724		109.47
O-Si-O/O_b	2.09724		109.47

Table 1: Potential parameters describing the zeolite-zeolite interactions, where O_b and H_b are the hydroxyl oxygen and hydrogen respectively.

The potentials describing the interaction between methanol and the zeolite framework were also adapted by Plant et al. from the work of Blanco and Auerbach and were scaled slightly from the original parameters. The original values were obtained from the CVFF force field and were adjusted to fit heats of adsorption in faujasites [71] and other zeolites,[72-74] and also PFG-NMR diffusion coefficient measurements in MFI zeolites.[75] Said parameters were derived for methanol diffusion in siliceous faujasites rather than HY. For this reason

the potentials describing the interaction of methanol with the acidic bridging framework hydroxyl were taken from the work of Kiselev[76] Vetrival et al.[77] implemented and listed in work by Shubin and Catlow,[78] investigating butanol isomer behaviour in H-ZSM-5.

Atomic Charges			
Species	**Charge (a.u.)**		
C	-0.093		
H	0.1		
O_{MeOH}	-0.432		
H_{MeOH}	0.225		
Intramolecular Potentials			
Bonds	**k (eV Å^{-2})**	**Length (Å)**	
C-H	29.56	1.105	
C-O_{MeOH}	33.33	1.420	
H-O_{MeOH}	46.97	0.945	
Angles	**k eV (rad^{-2})**	**θ(˚)**	
C-O_{MeOH}-H_{MeOH}	5.6	108.32	
H-C-O_{MeOH}	5.5	106.90	
H-C-H	4.4	108.38	
Dihedrals	**K(eV)**	**A**	**β**
H-C-O_{MeOH}-H_{MeOH}	0.00762	1.0	3.0

Table 2: Potential parameters describing intramolecular methanol interactions, where O_{MeOH} and H_{MeOH} are the methanol hydroxyl oxygen and hydrogen respectively.

Methanol-Zeolite Interactions		
Atoms	**ϵ (eV)**	**σ (Å)**
O/O_b--H_{MeOH}	0.004987	2.557
O/O_b--O_{MeOH}	0.010545	2.764
O/O_b--C	0.006594	2.958
O/O_b--H	0.004987	2.557
O/O_b--C	0.00828	3.150
H_b--H_{MeOH}	0.000851	1.784
H_b-- O_{MeOH}	0.00338	2.920
H_b--C	0.00299	2.806
H_b--H	0.000851	1.784

Table 3: Lennard-Jones potential parameters describing methanol-zeolite interactions.

Methanol-Methanol Interactions		
Atoms	**ϵ (eV)**	**σ (Å)**
H—H/H_{MeOH}	0.00165	2.450
H--C	0.00338	2.920
H--O_{MeOH}	0.00404	2.650
O_{MeOH}- -O_{MeOH}	0.00988	2.860
O_{MeOH}--C	0.00828	3.150
O_{MeOH}--H_{MeOH}	0.00404	2.650
C-- H_{MeOH}	0.00338	2.920

Table 4: Lennard-Jones potential parameters describing methanol-methanol interactions.

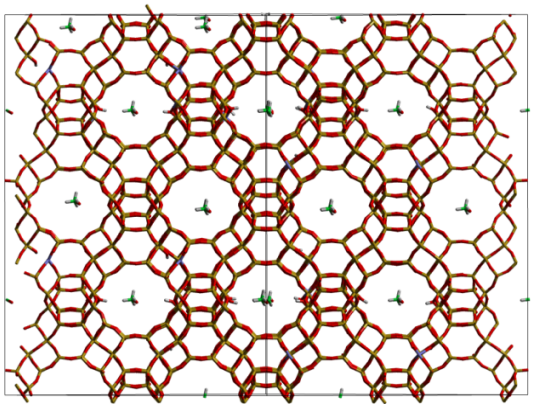

Fig 2. Pre-equillibriation configuration of the MD simulation of methanol in HY

The methanol molecules were placed in the centre of the faujasite supercages in the supercell, avoiding close contact with the channel walls. The loadings of 6 molecules per unit cell were chosen to match those of the experiment. An example of the starting configuration is shown in figure 2. The system was then equilibrated at the desired temperature for 1 ns in the canonical (NVT) ensemble. A Berendsen[79] thermostat was used to maintain the temperature constant, with a time constant for thermal energy exchange set at 1 ps. This thermostatting procedure has led to successful and stable equilibration in previous work[28-30,80] After the equilibration run, the production run of 10 ns in the microcanonical (NVE) ensemble was carried out at 300, 330, 360 and 400 K. A timestep of 0.5 fs was used and the atomic coordinates were saved every picosecond (every 2000 steps). All simulations were carried out using the DL_POLY_4 code[81]. The production time of 10 ns was chosen because it was sufficient to obtain true diffusive motion, illustrated by a linear mean square displacement (MSD) plot. The carbon atom of each molecule then had its coordinates logged, allowing self-diffusion coefficients to be calculated from the Einstein relationship.

3. Results and Discussion

3.1 Quasielastic Neutron Scattering

QENS spectra at 360 K at each temperature are shown at 4 Q values in figure 3. The spectra are fitted to a delta function convoluted with the resolution measurement taken at 6 K, a single Lorentzian function (which was enough of describe the data satisfactorily) and a flat background function. The Lorentzian component is consistently broadening with Q at all temperatures.

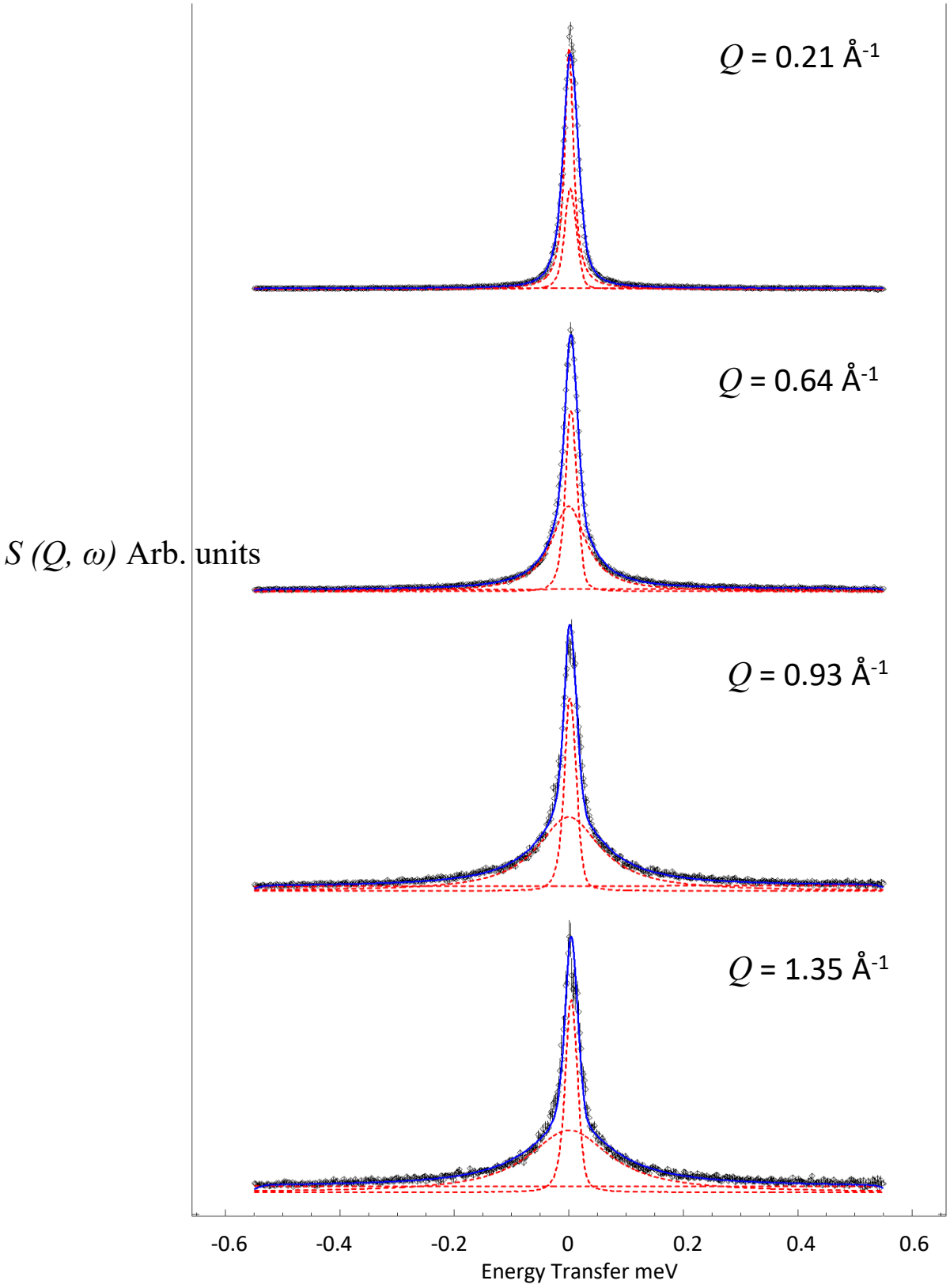

Fig 3. S(Q,ω) at 4 Q values for methanol in HY at 360 K. (--) represents the total fit, (--) represent the resolution function, the Lorentzian component and the flat background. A single Lorentzian quasielastic component is observable.

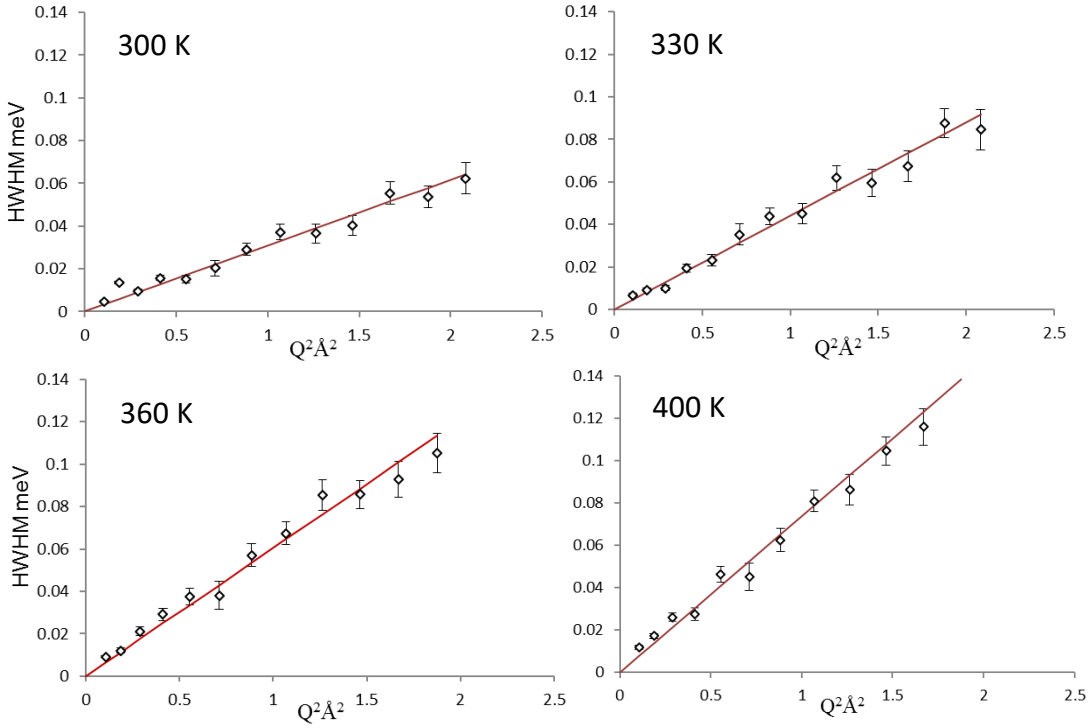

Fig 4. Q dependencies of the HWHM of the Lorentzian component of each QENS spectrum for methanol in HY at all 4 temperatures. The linear dependence with Q^2 suggests Fickian diffusion.

The Q dependencies of the HWHM of the Lorentzian component are plotted for all temperatures in figure 4. A linear dependence of the HWHM with Q^2 is adhered to at all four temperatures, indicative of Fickian diffusion. The error in the neutron data points in figure 3 are assigned based on Poisson statistics, while the error in the Lorentzian HWHM fits (figure 4) are assigned using a Monte Carlo method where data sets are generated virtually within the neutron data point error bars and then fitted. The measured diffusion coefficients are in a range of 2–5 x 10^{-10} m^2s^{-1} and are listed in table 4 and plotted in figure 5.

The Arrhenius dependence, plotted in figure 6 gives an activation energy of 8.8 kJ mol^{-1}. We note that the D_S values obtained by QENS are higher by an order of magnitude than all experimental diffusion coefficients measured of methanol in NaX (Si/Al = 1.2) and MD studies in NaY (Si/Al = 2.4). This observation may be attributed to the high concentration of counterions throughout the structure of low silica NaY which may be hindering diffusion. These extra framework counterions are not present in HY, which instead has bridging hydroxyls attached to the framework.

T K	QENS (present work)	MD (present work)	MD in siliceous Y (ref 48)	MD in NaX (ref 48)	PFG-NMR NaX (ref 46)	Tracer ZLC in NaX (ref 47)
300	2.05×10^{-10} $\pm 0.32 \times 10^{-10}$	1.61×10^{-9}	-	-	-	-
330	2.9×10^{-10} $\pm 0.56 \times 10^{-10}$	2.15×10^{-9}	-	-	-	-
350	-	-	8×10^{-9}	-	-	-
360	4×10^{-10} $\pm 0.93 \times 10^{-10}$	2.68×10^{-9}	-	-	-	-
373	-	-	-	-	6×10^{-11}	7×10^{-11}
400	4.9×10^{-10} $\pm 1.2 \times 10^{-10}$	3.21×10^{-9}	1×10^{-8}	4.7×10^{-11}	-	-
Ea kJ mol^{-1}	8.8	6.9	5.8	24	14	-

Table 4. Self-diffusion coefficients (D_s) of methanol in HY and activation energies of diffusion (Ea) measured from the current study in comparison with previous studies of other faujasite systems.

The less hindered diffusion in HY is also illustrated by the lower activation energy of diffusion from our QENS studies than from the experimental studies and MD simulations in NaX. We note also that our QENS measurements result in diffusion coefficients that are lower than those obtained previous MD simulations in siliceous faujasite by a factor of 20 at ~360 K and 400 K. This discrepancy is reasonable given the lack of proton sites in the siliceous MD simulation, removing the potential for favorable H-bonding between the methanol OH groups and the Brønsted acid sites (or terminal hydroxyls) present in the aluminated structure. The removal of this H-bonding potential is also combined with the use of a perfect zeolite crystal in the simulations, where defects and grain boundaries on the scale of a few nanometers would exist in the experimental sample, contributing additionally to the observed discrepancy. Importantly, the methanol loading is not the same for our QENS studies and the previous MD simulations (6 molecules per unit cell and 8 molecules per unit cell respectively). The H-bonding capability is further illustrated in our MD simulations reported in 3.2.

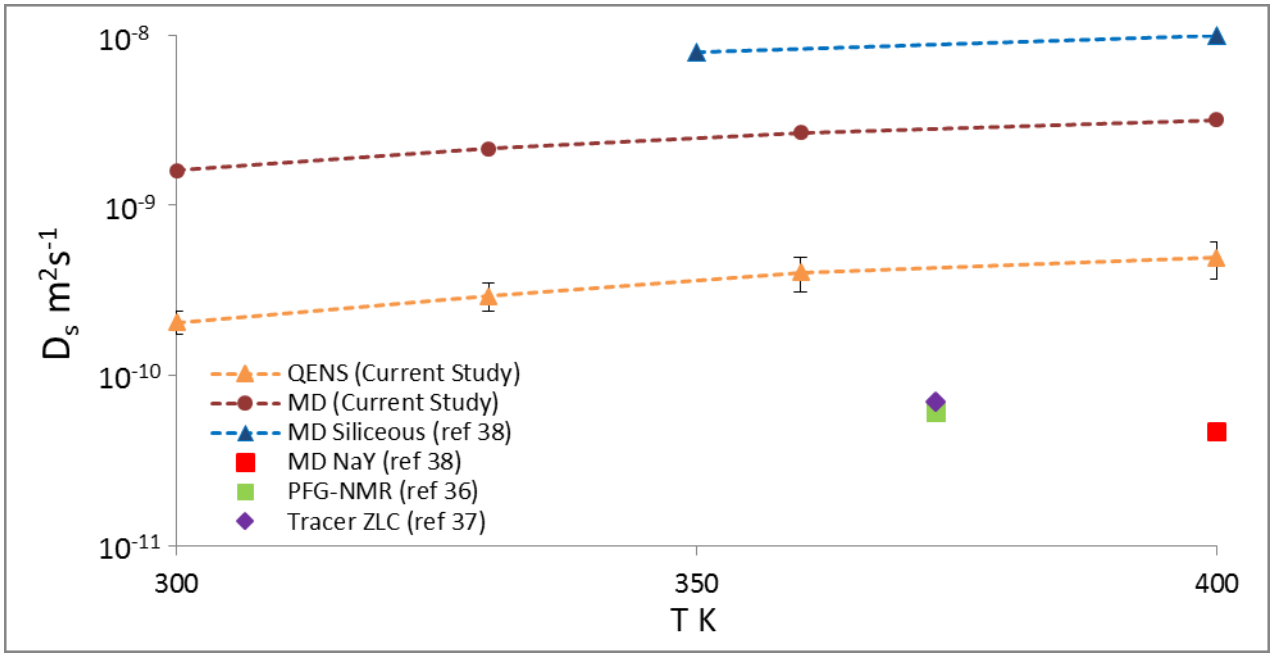

Fig. 5. Plot of diffusion coefficients of methanol in different faujasite systems between 300 – 400 K measured using different methods, including the QENS and MD measurements in the current study.

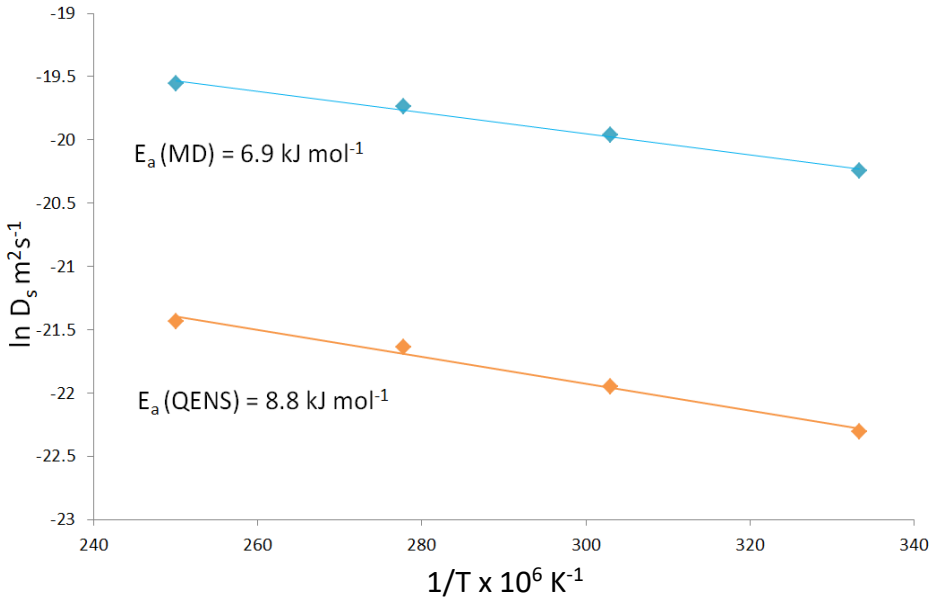

Fig. 6. Arrhenius plots and calculated Ea for methanol in HY from diffusion coefficients measured by QENS and MD.

3.2 Molecular Dynamics Simulations

The mean squared displacement (MSD) plots at each temperature are shown in figure 7, we note that the linearity of each plot confirms that our statistics are sufficient in calculating the self-diffusivity. Calculated D_s values are listed in table 5.

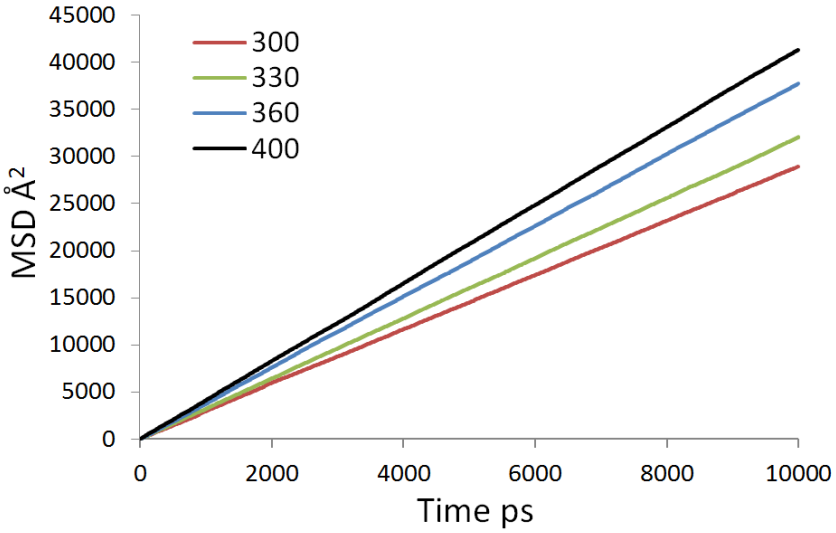

Fig 7. MSD plots at each temperature for methanol in HY.

With regard to our QENS experiments, our calculated D_s values are higher by a factor of 7.8, 7.4, 6.7 and 6.5 with each increasing temperature. The calculated values are expected to be at the upper limit of experiment due to the use of a perfect crystal with evenly distributed Brønsted acid sites and the discrepancy is of a magnitude similar to those shown for *n*- and isoalkanes in silicalite.[28,30] The defects may be particularly significant upon comparison with our high silica HY sample, which as noted previously[35] was synthesized through steam dealumination, which would leave significant defects such as silanol nests which may act as strong methanol adsorption sites, hindering diffusion. The hindrance may also be illustrated by the higher activation energy measured by QENS, higher by ~2 kJ mol^{-1} potentially due to the additional energy necessary to overcome the binding energy to silanol nests or other defects such as extraframework aluminum, or grain boundaries on the nanoscale.

With respect to previous simulations, our calculated diffusion coefficients are lower than those obtained in the siliceous structure,[38] by roughly a factor of 3 at 400 K, with an activation energy higher by 1.1 kJ mol^{-1}. This observation is sensible due to the presence of Brønsted acid sites in our simulated zeolite structure, allowing for favourable H-bonding interactions between the acid sites and the methanol molecules slowing diffusion. Examples of these observed H-bonds are shown in figure 8, showing both end-on and side-on geometries as observed to be stable configurations in previous studies.[82-84]

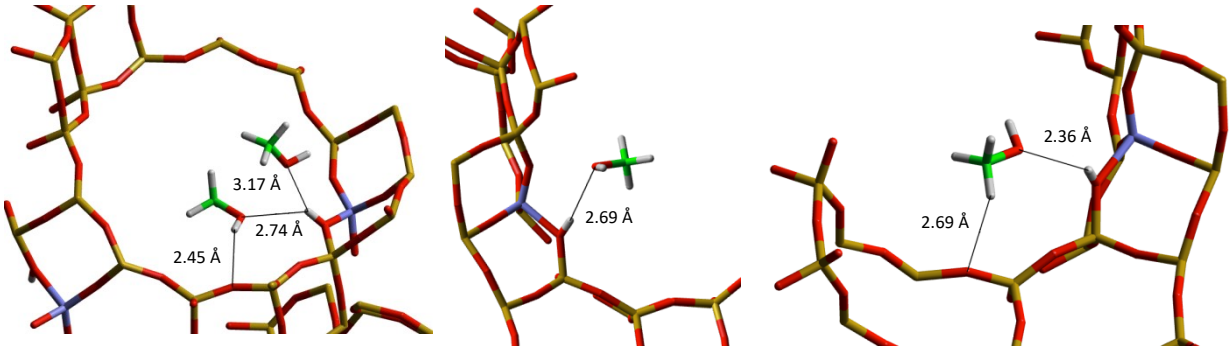

Fig 8. Typical H-bonded configurations of methanol in HY exhibiting both end-on and side-on geometry.

We note that the bond lengths are similar to those seen in reference 38 for NaX. However, the diffusion coefficients calculated in NaX are lower by a factor of 68 than our simulated HY system (1 order of magnitude lower than our experiment). The NaX Si/Al ratio in reference 38 was 2.4, compared to 30 in our study. This far higher population of Na^+ coordination sites would explain the significant reduction in methanol mobility, further illustrated by the activation energy of 24 kJ mol^{-1} (compared to 6.9 and 8.8 kJ mol^{-1} for our simulated and experimental HY systems respectively).

From figure 5 we observe a logical trend in measured diffusivities given the systems under study, and the methods used when studying methanol in faujasite systems. The highest diffusivities are calcuated when using MD simulations in the siliceous structure, as the coordination sites acting as potential barriers for diffusion are not present as in the other systems. The second highest diffusivities are observed by our MD simulations in the HY structure, slower than the referenced siliceous simulations due to H-bonding observed between the methanol and the Brønsted acid sites. The third highest diffusivities are measured in the HY structure using QENS, we expect this as MD simulations usually yield

higher diffusivities than experiment due to the use of a perfect crystal as previously mentioned. Again, this factor is particularly significant in our comparison as our experimental samples were brought to this composition through steam dealumination, leaving defects such as silanol nests throughout the crystal structure which may act as an adsorption trap for methanol molecules, slowing their diffusion further. The slowest diffusivities are measured in NaX, with similar values obtained using PFG-NMR and tracer ZLC in methods[36,37] and MD simulations in reference 38, where the high concentration of counterions (Si/Al = 1.2 in the experiments and 2.4 for the MD simulations) slow diffusion through strong interactions of the methanol oxygen with the counterion.

4. Summary and Conclusions

We have reported the microscopic measurement of methanol diffusion in zeolite HY using QENS experiments and MD simulations. Measurements between 300 – 400 K gave experimental diffusion coefficients in the range of 2–5 x 10^{-10} m^2s^{-1} giving an activation energy of 8.8 kJ mol^{-1}, and theoretical diffusion coefficients of 1.6–3.2 x 10^{-9} m^2s^{-1} giving an activation energy of 6.9 kJ mol^{-1} . The discrepancy is of a magnitude previously observed between these methods for similar systems, and attributed primarily to defects in the experimental sample related to its synthesis method. The measurements in HY are lower than those obtained by simulations in siliceous faujasite due to favourable H-bonding interactions between methanol and framework bridging hydroxyls as observed in the MD simulations. Our experimental and theoretical measurements are all significantly higher than previous studies of methanol diffusion in NaX (higher by a factor of 68 in when comparing simulations), attributed to the lower concentration of extraframework cations in the zeolite framework. The study highlights the power of combined theoretical and experimental microscopic studies in probing the effect of zeolite composition on diffusion of catalytically relevant species in microporous catalysts.

References

(1) Olsbye, U.; Svelle, S.; Bjørgen, M.; Beato, P.; Janssens, T. V.; Joensen, F.; Bordiga, S.; Lillerud, K. P. *Angewandte Chemie International Edition* **2012**, *51*, 5810.

(2) Hemelsoet, K.; Van der Mynsbrugge, J.; De Wispelaere, K.; Waroquier, M.; Van Speybroeck, V. *ChemPhysChem* **2013**, *14*, 1526.

(3) Kvisle, S.; Fuglerud, T.; Kolboe, S.; Olsbye, U.; Lillerud, K. P.; Vora, B. V. *Handbook of heterogeneous catalysis* **2008**.

(4) Stöcker, M. *Microporous and Mesoporous Materials* **1999**, *29*, 3.

(5) Borgna, A.; Sepulveda, J.; Magni, S.; Apesteguia, C. *Applied Catalysis A: General* **2004**, *276*, 207.

(6) Venuto, P. B.; Habib Jr, E. T. **1979**.

(7) Vogt, E.; Weckhuysen, B. *Chemical Society Reviews* **2015**, *44*, 7342.

(8) Wieland, W. S.; Davis, R. J.; Garces, J. M. *Journal of Catalysis* **1998**, *173*, 490.

(9) Palomares, A.; Eder-Mirth, G.; Rep, M.; Lercher, J. *Journal of Catalysis* **1998**, *180*, 56.

(10) Fei, J.; Hou, Z.; Zhu, B.; Lou, H.; Zheng, X. *Applied Catalysis A: General* **2006**, *304*, 49.

(11) Jin, D.; Zhu, B.; Hou, Z.; Fei, J.; Lou, H.; Zheng, X. *Fuel* **2007**, *86*, 2707.

(12) Bull, L. M.; Henson, N. J.; Cheetham, A. K.; Newsam, J. M.; Heyes, S. J. *The Journal of Physical Chemistry* **1993**, *97*, 11776.

(13) Eic, M.; Goddard, M.; Ruthven, D. *Zeolites* **1988**, *8*, 327.

(14) Jobic, H.; Fitch, A. N.; Combet, J. *The Journal of Physical Chemistry B* **2000**, *104*, 8491.

(15) Shen, D.; Rees, L. V. *Zeolites* **1991**, *11*, 666.

(16) Jobic, H.; Bee, M.; Kearley, G. J. *The Journal of Physical Chemistry* **1994**, *98*, 4660.

(17) Deroche, I.; Maurin, G.; Borah, B.; Yashonath, S.; Jobic, H. *The Journal of Physical Chemistry C* **2010**, *114*, 5027.

(18) Auerbach, S. M.; Henson, N. J.; Cheetham, A. K.; Metiu, H. I. *The Journal of Physical Chemistry* **1995**, *99*, 10600.

(19) Auerbach, S. M.; Metiu, H. I. *The Journal of chemical physics* **1996**, *105*, 3753.

(20) Clark, L. A.; George, T. Y.; Gupta, A.; Hall, L. L.; Snurr, R. Q. *The Journal of chemical physics* **1999**, *111*, 1209.

(21) Klein, H.; Kirschhock, C.; Fuess, H. *The Journal of Physical Chemistry* **1994**, *98*, 12345.

(22) Sanborn, M. J.; Snurr, R. Q. *Separation and purification technology* **2000**, *20*, 1.

(23) Saravanan, C.; Auerbach, S. M. *The Journal of chemical physics* **1997**, *107*, 8132.

(24) Yashonath, S. *The Journal of Physical Chemistry* **1991**, *95*, 5877.

(25) Yashonath, S.; Santikary, P. *The Journal of Physical Chemistry* **1994**, *98*, 6368.

(26) Demontis, P.; Yashonath, S.; Klein, M. L. *The Journal of Physical Chemistry* **1989**, *93*, 5016.

(27) Jobic, H.; Theodorou, D. N. *Microporous and mesoporous materials* **2007**, *102*, 21.

(28) O'Malley, A. J.; Catlow, C. R. A. *Physical Chemistry Chemical Physics* **2013**, *15*, 19024.

(29) O'Malley, A. J; Catlow, C. *Physical Chemistry Chemical Physics* **2015**, *17*, 1943.

(30) O'Malley, A. J.; Catlow, C. R. A.; Monkenbusch, M.; Jobic, H. *The Journal of Physical Chemistry C* **2015**, *119*, 26999.

(31) Jobic, H. *Journal of Molecular Catalysis A: Chemical* **2000**, *158*, 135.

(32) Jobic, H.; Theodorou, D. N. *The Journal of Physical Chemistry B* **2006**, *110*, 1964.

(33) Rep, M.; Palomares, A.; Eder-Mirth, G.; Van Ommen, J.; Rösch, N.; Lercher, J. *The Journal of Physical Chemistry B* **2000**, *104*, 8624.

(34) Schenkel, R.; Jentys, A.; Parker, S. F.; Lercher, J. A. *The Journal of Physical Chemistry B* **2004**, *108*, 7902.

(35) O'Malley, A. J.; Parker, S. F.; Chutia, A.; Farrow, M. R.; Silverwood, I. P.; García-Sakai, V.; Catlow, C. R. A. *Chemical Communications* **2016**.

(36) Meunier, F.; Gray, P.; Kärger, J.; Xu, Z.; Ruthven, D. *Zeolites* **1994**, *14*, 242.
(37) Brandani, S.; Ruthven, D. M. *Zeolites* **1995**, *15*, 494.
(38) Plant, D.; Maurin, G.; Bell, R. *The Journal of Physical Chemistry B* **2006**, *110*, 15926.
(39) Plant, D. F.; Maurin, G.; Bell, R. G. *The Journal of Physical Chemistry B* **2007**, *111*, 2836.
(40) Maurin, G.; Plant, D.; Henn, F.; Bell, R. G. *The Journal of Physical Chemistry B* **2006**, *110*, 18447.
(41) Nanok, T.; Vasenkov, S.; Keil, F. J.; Fritzsche, S. *Microporous and Mesoporous Materials* **2010**, *127*, 176.
(42) DeCanio, S. J.; Sohn, J. R.; Fritz, P. O.; Lunsford, J. H. *Journal of Catalysis* **1986**, *101*, 132.
(43) Nováková, J.; Kubelková, L.; Dolejšek, Z. *Journal of Catalysis* **1987**, *108*, 208.
(44) Jobic, H.; Renouprez, A.; Bee, M.; Poinsignon, C. *The Journal of Physical Chemistry* **1986**, *90*, 1059.
(45) Mitra, S.; Kamble, V.; Tripathi, A.; Gupta, N.; Mukhopadhyay, R. *Pramana* **2004**, *63*, 443.
(46) Sharma, V.; Gautam, S.; Mitra, S.; Mukhopadhyay, R. *Zeitschrift für Physikalische Chemie International journal of research in physical chemistry and chemical physics* **2010**, *224*, 133.
(47) Jobic, H.; Bée, M.; Pouget, S. *The Journal of Physical Chemistry B* **2000**, *104*, 7130.
(48) Millot, B.; Méthivier, A.; Jobic, H.; Moueddeb, H.; Bée, M. *The Journal of Physical Chemistry B* **1999**, *103*, 1096.
(49) Mitra, S.; Tripathy, A.; Gupta, N.; Mukhopadhyay, R. *Applied Physics A* **2002**, *74*, s1308.
(50) Rezaei, P. S.; Shafaghat, H.; Daud, W. M. A. W. *RSC Advances* **2015**, *5*, 65408.
(51) Hu, E.; Hu, Y.; Cheng, H. *Journal of hazardous materials* **2015**, *299*, 444.
(52) Telling, M. T.; Andersen, K. H. *Physical Chemistry Chemical Physics* **2005**, *7*, 1255.
(53) Azuah, R. T.; Kneller, L. R.; Qiu, Y.; Tregenna-Piggott, P. L.; Brown, C. M.; Copley, J. R.; Dimeo, R. M. *Journal of Research of the National Institute of Standards and Technology* **2009**, *114*, 341.
(54) Hriljac, J.; Eddy, M.; Cheetham, A.; Donohue, J.; Ray, G. *Journal of Solid State Chemistry* **1993**, *106*, 66.
(55) Dempsey, E.; Kühl, G.; Olson, D. H. *The Journal of Physical Chemistry* **1969**, *73*, 387.
(56) Ghysels, A.; Moors, S. L.; Hemelsoet, K.; De Wispelaere, K.; Waroquier, M.; Sastre, G.; Van Speybroeck, V. *The Journal of Physical Chemistry C* **2015**, *119*, 23721.
(57) Nicholas, J. B.; Hopfinger, A. J.; Trouw, F. R.; Iton, L. E. *Journal of the American Chemical Society* **1991**, *113*, 4792.
(58) Demontis, P.; Suffritti, G. B.; Quartieri, S.; Fois, E. S.; Gamba, A. *The Journal of Physical Chemistry* **1988**, *92*, 867.
(59) García-Sánchez, A.; Dubbeldam, D.; Calero, S. *The Journal of Physical Chemistry C* **2010**, *114*, 15068.
(60) Hill, J.-R.; Sauer, J. *The Journal of Physical Chemistry* **1995**, *99*, 9536.
(61) Schröder, K.-P.; Sauer, J.; Leslie, M.; Richard, C.; Catlow, A.; Thomas, J. M. *Chemical physics letters* **1992**, *188*, 320.
(62) Jackson, R.; Catlow, C. *Molecular Simulation* **1988**, *1*, 207.
(63) Youngs, T. *Journal of computational chemistry* **2010**, *31*, 639.
(64) Blanco, C.; Auerbach, S. M. *The Journal of Physical Chemistry B* **2003**, *107*, 2490.
(65) Allinger, N. L.; Rahman, M.; Lii, J. H. *Journal of the American Chemical Society* **1990**, *112*, 8293.
(66) Serrallach, A.; Meyer, R.; Günthard, H. H. *Journal of Molecular Spectroscopy* **1974**, *52*, 94.
(67) Lees, R.; Baker, J. *The Journal of Chemical Physics* **1968**, *48*, 5299.

(68) Ivash, E. V.; Dennison, D. M. *The Journal of Chemical Physics* **1953**, *21*, 1804.

(69) Kimura, K.; Kubo, M. *The Journal of Chemical Physics* **1959**, *30*, 151.

(70) Dauber-Osguthorpe, P.; Roberts, V. A.; Osguthorpe, D. J.; Wolff, J.; Genest, M.; Hagler, A. T. *Proteins: Structure, Function, and Bioinformatics* **1988**, *4*, 31.

(71) Izmailova, S.; Karetina, I.; Khvoshchev, S.; Shubaeva, M. *Journal of colloid and interface science* **1994**, *165*, 318.

(72) Nayak, V.; Moffat, J. *The Journal of Physical Chemistry* **1988**, *92*, 7097.

(73) Thamm, H. *Journal of the Chemical Society, Faraday Transactions 1: Physical Chemistry in Condensed Phases* **1989**, *85*, 1.

(74) Pope, C. G. *Journal of the Chemical Society, Faraday Transactions* **1993**, *89*, 1139.

(75) Caro, J.; Bülow, M.; Richter-Mendau, J.; Kärger, J.; Hunger, M.; Freude, D.; Rees, L. V. *Journal of the Chemical Society, Faraday Transactions 1: Physical Chemistry in Condensed Phases* **1987**, *83*, 1843.

(76) Kiselev, A.; Lopatkin, A.; Shulga, A. *Zeolites* **1985**, *5*, 261.

(77) Vetrivel, R.; Catlow, C.; Colbourn, E. *The Journal of Physical Chemistry* **1989**, *93*, 4594.

(78) Shubin, A. A.; Catlow, C. R. A.; Thomas, J. M.; Zamaraev, K. I. In *Proceedings of the Royal Society of London A: Mathematical, Physical and Engineering Sciences*; The Royal Society: 1994; Vol. 446, p 411.

(79) Berendsen, H. J.; Postma, J. P. M.; van Gunsteren, W. F.; DiNola, A.; Haak, J. *The Journal of chemical physics* **1984**, *81*, 3684.

(80) Runnebaum, R. C.; Maginn, E. J. *The Journal of Physical Chemistry B* **1997**, *101*, 6394.

(81) Todorov, I. T.; Smith, W.; Trachenko, K.; Dove, M. T. *Journal of Materials Chemistry* **2006**, *16*, 1911.

(82) Zicovich-Wilson, C.; Viruela, P.; Corma, A. *The Journal of Physical Chemistry* **1995**, *99*, 13224.

(83) Blaszkowski, S.; Van Santen, R. *The Journal of Physical Chemistry* **1995**, *99*, 11728.

(84) O'Malley, A. J.; Logsdail, A. J.; Sokol, A. A.; Catlow, C. R. A. *Faraday Discussions* **2016**.